AD-A098 624 NAVAL RESEARCH LAB WASHINGTON DC F/G 9/5
MIXED SLOW WAVE OPERATION OF A WIDE BAND DIELECTRIC GYROTRON.(U)
MAY 81 J CHOE, H UHM, S AHN
UNCLASSIFIED NRL-MR-4510 NL

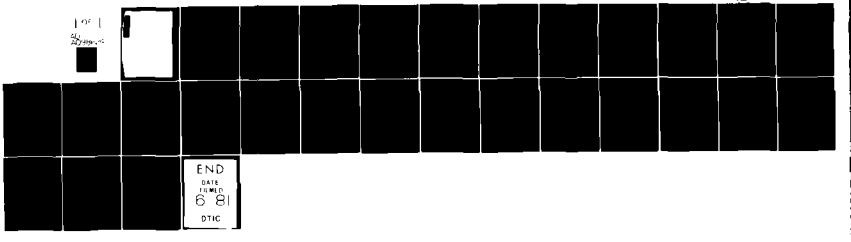

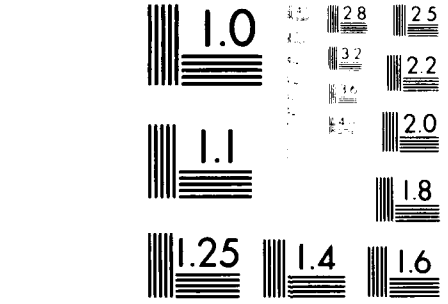

45

SECURITY CLASSIFICATION OF THIS PAGE (When Data Entered)

REPORT DOCUMENTATION PAGE	READ INSTRUCTIONS BEFORE COMPLETING FORM
1. REPORT NUMBER: NRL Memorandum Report 4510	2. GOVT ACCESSION NO. AD-A098424 / 3. RECIPIENT'S CATALOG NUMBER
4. TITLE (and Subtitle): MIXED SLOW WAVE OPERATION OF A WIDE BAND DIELECTRIC GYROTRON	5. TYPE OF REPORT & PERIOD COVERED: Interim report on a continuing NRL problem.
	6. PERFORMING ORG. REPORT NUMBER
7. AUTHOR(s): J. Choe*, H. Uhm*, and S. Ahn	8. CONTRACT OR GRANT NUMBER(s)
9. PERFORMING ORGANIZATION NAME AND ADDRESS: Naval Research Laboratory, Washington, DC 20375	10. PROGRAM ELEMENT, PROJECT, TASK AREA & WORK UNIT NUMBERS: 68-0755-0-1; NAVELEX; NSWC IR&D Funds
11. CONTROLLING OFFICE NAME AND ADDRESS	12. REPORT DATE: May 1981
	13. NUMBER OF PAGES: 28
14. MONITORING AGENCY NAME & ADDRESS(if different from Controlling Office)	15. SECURITY CLASS. (of this report): UNCLASSIFIED
	15a. DECLASSIFICATION/DOWNGRADING SCHEDULE

16. DISTRIBUTION STATEMENT (of this Report)

Approved for public release; distribution unlimited.

17. DISTRIBUTION STATEMENT (of the abstract entered in Block 20, if different from Report)

18. SUPPLEMENTARY NOTES

*Present address: Naval Surface Weapons Center, White Oak, MD 20910

19. KEY WORDS (Continue on reverse side if necessary and identify by block number)

Gyrotron
Cyclotron maser instability
Velocity spread
Slow wave structure
Dielectric waveguide
Wide band amplifier

20. ABSTRACT (Continue on reverse side if necessary and identify by block number)

The bandwidth broadening effect of mixing two slow wave modes in a dielectric loaded gyrotron is investigated for a small axial momentum spread. The usual intermediate wavelength model (IWM) combines with the short wavelength mode (SWM) by reducing the electron beam radius and creates a mixed slow wave. The resulting bandwidth for the mixed mode gyrotron becomes at least twice broader than that for the pure IWM at the small velocity spread ($\lesssim 1\%$) with a substantial contribution of the SWM. Moreover, the mixed mode operation can allow up to several times more power than the usual IWM-mode operation.

(about but less than 1%)

DD FORM 1 JAN 73 1473 EDITION OF 1 NOV 65 IS OBSOLETE S/N 0102-014-6601

SECURITY CLASSIFICATION OF THIS PAGE (When Data Entered)

CONTENTS

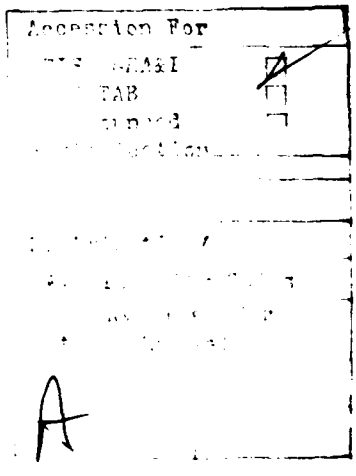

MIXED SLOW WAVE OPERATION OF A WIDE BAND DIELECTRIC GYROTRON

I. INTRODUCTION

A recent paper[1] investigates the stability behavior of a dielectric loaded gyrotron for wide band applications. (The dielectric constant is ε. We use the C.G.S. unit system in this paper.) The Doppler-shifted electron cyclotron mode for the azimuthally symmetric, transverse electric (TE) perturbation is found to exhibit three unstable branches characterized by their phase velocities (v_{ph}); the long wavelength mode (LWM, $v_{ph} > c$), the intermediate wavelength mode (IWM, $c > v_{ph} > c\varepsilon^{-1/2}$), and the short wavelength mode (SWM, $v_{ph} < c\varepsilon^{-1/2}$). The wide band capability and its corresponding optimum conditions for each mode have been determined in terms of the axial momentum spread. For parameters of a typical gyrotron [see Eq. (8)], it is found that for a small axial momentum spread ($\lesssim$ 1%), a bandwidth in excess of 40% is possible for the slow waves (IWM and SWM), whereas for a larger spread ($\gtrsim$ 5%) the fast wave (LWM) is desirable with a 10% bandwidth. It is, therefore, concluded that the bandwidth and the choice of the operating mode are primarily determined by the axial momentum spread of the beam electron.

In view of encouraging recent works[2] on the electron gun study, which report less than 1% of the axial momentum spread (neglecting the effects of the cathode surface roughness), the slow wave (IWM, SWM) operations for the gyrotron appear to be very advantageous. However, previous theoretical studies of the wide band gyrotron have been restricted to one of two slow waves, either the IWM[1-3] or the SWM,[1] mainly due to the different optimization conditions for the two modes.[1] In this paper, we will develop a unified theory of these two modes where the combined bandwidth is broader than that of each mode. The present work extends the previous theory[1] developed by the

Manuscript submitted March 17, 1981.

authors, which predicts the coexistence of the SWM with the IWM. The relevant parameter for the mode mixing is found to be the beam location. By reducing the beam radius from the inner radius of the dielectric material toward the waveguide axis, the contribution of the SWM to instability is greatly enhanced whereas that of the IWM is somewhat diminished. The combined effect results in a broader instability bandwidth. However, the growth rate of instability is slightly reduced.

Some nuisances in a dielectric loaded microwave device seem to be intense dielectric heating[2] and the dielectric surface charging. Since the perturbed fields of the IWM mode tend to concentrate inside the dielectric layer, and thus the beam location is optimized near the dielectric wall, the high power microwave amplification via the IWM mode is somewhat limited, indeed. Results of our analysis will indicate that the field energy in the mixed mode operation is greatly reduced in the dielectric layer by reducing the beam radius. The increased participation of the SWM is responsible for this energy reduction. As pointed out in Ref. 1 and as will be shown in Sec. IV, the SWM is driven by the highly localized fields at the beam location, (also see Appendix) thereby decreasing field concentration within the dielectric layer. The mixture of the SWM, therefore, provides both the enhanced bandwidth and the reduction of the field energy in the dielectric layer.

A brief review of the derivation of the dispersion relation and the characteristics of the unstable modes is given in Sec. II. In Sec. III, the mixed mode operation is discussed in terms of the bandwidth and the growth rate. The perturbed field profile is examined in Sec. IV in order to explain the mode mixing. Special emphasis is given on the contribution of the SWM to instability and the field energy contained in the dielectric. We

point out that the analysis in this paper explicitly assumes the optimistically small axial momentum spread (1%). A schematic physical model for the SWM instability is discussed in the Appendix.

II. DISPERSION RELATION AND MODE CHARACTERISTICS

The cross section of the dielectric gyrotron is shown in Fig. 1. The dielectric material with its dielectric constant ε is filled from its inner radius R_w to the outer conducting wall at R_c. The hollow electron beam is confined between R_- and R_+ with its center at R_o as shown in Fig. 1. The cylindrical coordinates (r, θ, z) are used.

Since the details of the procedures in obtaining the dispersion relation are given in Ref. 1, we will only present the outline. The dispersion relation is derived within the framework of the Maxwell-Vlasov system for the fields, $\underline{E}(\underline{x}, t)$ and $\underline{B}(\underline{x}, t)$, and the beam electron distribution function $f(\underline{x}, \underline{p}, t)$. Further, any quantity Ψ is linearized according to

$$\Psi(\underline{x},t) = \Psi_o(r) + \Psi_1(r) \exp[i(kz-\omega t)] \qquad (1)$$

with the equilibrium quantity Ψ_o and the small Fourier decomposed perturbation Ψ_1. Note that we limit our attention to the azimuthally symmetric perturbation with the frequency ω and the axial wave number k. Moreover, we will consider the transverse electric (TE) perturbation only. It is assumed that the beam is tenuous, and the beam thickness is small. The solutions for the perturbed fields in the beam-free regions are formally obtained (see Sec. IV), and the appropriate boundary conditions under the thin beam assumption connect these solutions. The contribution of the beam current is replaced by the jump condition on B_{z1} across the beam, while the amount of the jump is computed by the integration of the perturbed beam current via the moment equation of the perturbed distribution function. The perturbed distribution function, in turn, is obtained by the equilibrium orbit integral

with help of the tenuous beam assumption. In this method of the wave impedance matching[1,4] the field profile is not apriori given but results from the dispersion relation. Unlike the waveguide approximation,[5-7] this method is capable of predicting the short wavelength mode which does not originated from the beam-waveguide coupling (see Appendix). In order to examine the important effect of the axial momentum spread, the equilibrium distribution function f_o is assumed to be Lorentzian[1] in the axial momentum p_z, that is,

$$f_o \propto \hat{p}_z \Delta [(p_z - \hat{p}_z)^2 + \hat{p}_z^2 \Delta^2]^{-1} \tag{2}$$

Here $\hat{p}_z$ is the average axial momentum and Δ is the momentum spread ratio. The beam is assumed to be monoenergetic with γmc^2, and the average transverse (axial) velocity is given by $c\beta_\perp$ ($c\beta_z$). Finally, we obtain the linear dispersion relation for the azimuthally symmetric TE mode.[1]

$$B = \frac{B_N}{B_D} = - \frac{\nu \beta_\perp^2 c^2}{2\gamma R_o^2 [\omega - \omega_B + i|k| c\beta_z \gamma \Delta/\gamma_z^3]^2} \tag{3}$$

Here the Doppler-shifted beam mode ω_B is defined by

$$\omega_B = kc\beta_z + \omega_c/\gamma, \tag{4}$$

the wave admittance[1,4] B is given by

$$\begin{aligned} B_N &= 2B_1, \quad B_D = -\pi x_o^2 J_1(x_o) D, \\ D &= J_1(x_o) B_2 - N_1(x_o) B_1, \\ B_1 &= J_1(y_c) A_{NJ}(y_w, x_w) - N_1(y_c) A_{JJ}(y_w, x_w), \\ B_2 &= J_1(y_c) A_{NN}(y_w, x_w) - N_1(y_c) A_{JN}(y_w, x_w), \end{aligned} \tag{5}$$

and

$$A_{PQ}(y,x) \equiv y P_o(y) Q_1(x) - x Q_o(x) P_1(y), \tag{6}$$

where P and Q represent the Bessel function J or N. The arguments of the Bessel function are

$$x^2 \equiv (\omega^2/c^2 - k^2)\, r^2, \quad y^2 \equiv (\omega^2\varepsilon/c^2 - k^2)\, r^2 \tag{7}$$

and x_o, x_w and x_c are the values at $r=R_o$, R_w and R_c, respectively. In Eq. (3), $\nu \equiv Ne^2/mc^2$ is the Budker parameter, $\omega_c = eB_o/mc$ is the non-relativistic electron cyclotron frequency, and $\gamma_z = (1-\beta_z^2)^{-1/2}$ is the axial mass factor. Here N is the total number of electrons per unit axial length, (-e) and m are the charge and the rest mass of the electron, and c is the velocity of light. By noting that the unstable modes may occur near the beam mode ω_B, an approximate dispersion relation[1] for unstable modes is obtained as a cubic function in $\chi = \omega - \omega_B$.

In Fig. 2, a schematic gain (shown in dotted lines) vs. the axial wave-number k is plotted when the beam is cold [$\Delta = 0$, Eq. (2)]. Also shown for reference in Fig. 2 are the real frequencies (solid lines) for the beam mode ω_B [Eq. (4)], the dielectric waveguide mode ω_G [the solution of $B_N = 0$, Eq. (5)], the free space mode ck, and the free dielectric mode $ck/\varepsilon^{1/2}$. The beam mode ω_B intersects with ck and $ck/\varepsilon^{1/2}$ at $k_c = \omega_c/\gamma c(1-\beta_z)$ and $k_c' = \omega_c\, \varepsilon^{1/2}/\gamma\, c(1-\varepsilon^{1/2}\beta_z)$, respectively. The growth rate curve shows that the fast wave mode (the long wavelength mode) is separated from the two slow waves (the intermediate wavelength mode and the short wavelength mode) by a stable band near k_c. Both the LWM and the IWM are originated from the unstable coupling of the beam mode ω_B and the waveguide mode ω_G. On the other hand, the instability of the SWM is driven by the highly localized perturbed fields near the beam location[1] (see Sec. IV). Therefore, while both the LWM and the IWM may disappear depending on the dielectric parameters, the SWM is present regardless of these parameters. However, the growth rate due to the SWM is usually negligible in the IWM range. A simple physical model for the SWM instability is presented in the Appendix.

The reduction of the growth rate due to the axial momentum spread is the least for the LWM, moderate for the IWM, and the largest for the SWM. On the other hand, the bandwidth of the instability at small axial momentum spread is the broadest for the SWM, intermediate for the IWM, and the narrowest for the LWM. Throughout the remainder of this paper we assume the following beam parameters.

$$\beta_\perp = 0.4, \ \beta_z = 0.2, \ \nu = 0.002, \tag{8}$$

corresponding to the 60.3 kV of the anode voltage and 6.8 Amp. of the total axial current. For future reference, we also define

$$R_o^{\,o} = 2.017 \ c/\omega_c, \ R_c^{\,o} = 4.197 \ \ c/\omega_c. \tag{9}$$

It can be shown that $R_o^{\,o}$ and $R_c^{\,o}$ are the optimized beam center and the conducting wall location when the dielectric is absent.[1,4-7] With these parameters the optimization conditions for the wide band operation are found to be[1]: $\varepsilon \simeq 5$, $R_c/R_c^{\,o} \simeq 0.8$, $R_w/R_c = 0.7 \sim 0.8$, $R_o \to R_w$ for the LWM; $\varepsilon \simeq 15$, $R_c/R_c^{\,o} \simeq 0.6$, $R_w/R_c = 0.7 \sim 0.8$, $R_o \to R_w$ for the IWM; and $\varepsilon = 1$, $R_c/R_c^{\,o} \geq 1$, $R_o \to 0$ for the SWM. It is interesting to note that the optimization conditions for the IWM is different from those for the SWM. Especially we note that the IWM is optimized as the beam center R_o is placed as close as possible to the inner dielectric wall R_w, whereas R_o should decrease for the SWM. This competing nature provides a starting point for the mixed mode operation in an attempt to increase the bandwidth further by combining the two modes. This mixed mode operation via variation of the beam center location will be discussed in the next section. The proposed operation is only possible at small axial momentum spread (1%).

III. MIXED MODE OPERATION

In the previous section we have found that at small axial momentum spread (e.g., Δ=1%), either of the two slow wave modes, i.e., the IWM or

the SWM has a wide band capability. However, this individual mode (SWM) has intrinsic difficulties due to its instability driving mechanism. The IWM, which results from the beam-waveguide mode coupling, requires the beam center location (R_o) to be close to the dielectric inner wall (R_w), since the perturbed fields tend to concentrate in the dielectric layer. This concentration of the fields in the layer and the closeness of the beam to the inner wall location pose serious difficulties in the experimental setup. On the other hand, in the SWM utilization, it is extremely difficult to excite the wave initially, since the optimized SWM does not require a dielectric layer, and the natural propagation of the slow wave is impossible. However, each mode operation has a remedy for the difficulties of the other mode. The SWM, which arises from the highly localized fields at the beam location, not only reduces the field energy in the dielectric layer, but also demands the beam location to be away from the dielectric wall. Thus the difficulties associated with the IWM can be lessened by introducing the SWM. Meanwhile, the IWM, which needs a high ϵ dielectric layer, makes it possible to propagate a wide range of the slow waves, thereby providing the necessary initial input for the SWM operation. In this regard, the mixed mode gyrotron amplifier eliminates difficulties arising from the individual mode operations. Moreover, the instability bandwidth of the mixed mode operation is greatly enhanced. Evidently the relevant parameter for the mixed mode is the beam location.

In Fig. 3, the growth rates versus the axial wave number for the individually optimized IWM (solid lines) and the SWM (broken lines) are shown at several values of the axial momentum spread Δ. The beam parameters are those given in Eq. (8). Note the different optimized parameters for each mode, especially the beam center location R_o. For the IWM, R_o is close to R_w.

On the other hand, for the SWM, the beam radius R_o is placed as close to the axis as our theory allows.[1] Obviously at the limit of the practical axial momentum spread (Δ = 1%), the SWM exhibits the lower gain but wider bandwidth than the IWM. The IWM appears at a lower axial wave number than the SWM. In order to visualize the influence of the mode mixing, we examine the growth rates, retaining the IWM optimizing parameters [Fig. 3, ϵ = 15.2, R_c/R_c^o = 0.63, R_w/R_c^o = 0.53, Eq. (9)], but varying the beam radius R_o from R_o/R_o^o = 0.9 to R_o/R_o^o = 0.5. The growth rate curves for R_o variation are shown in Fig. 4(a). In Fig. 4(a) and in the remainder of this paper, the axial momentum spread (Δ) is assumed to be 1%. For R_o/R_o^o = 0.9, the mode is almost purely IWM. As the beam radius R_o is decreased, the contribution of the IWM to instability becomes smaller, and that of the SWM is increased. For R_o/R_o^o = 0.5 corresponding to the optimum SWM value (Fig. 3), almost the entire unstable range belongs to the SWM. In Fig. 4(b) the corresponding bandwidth and the maximum growth rate of the instability are illustrated in terms of R_o. The bandwidth is defined by the full width of the real frequency, at which the linear gain drops to exp(-1/2) of its maximum value,[8] normalized by its mean frequency $\bar{\omega}$. The maximum growth rate is also normalized by $\bar{\omega}$. The bandwidth increases from 46% for the pure IWM (R_o/R_o^o = 0.9, Fig. 3) to 90% for the mixed mode operation (R_o/R_o^o = 0.5). Out of 90% bandwidth for the mixed mode, 78% is from the SWM and 12% from the IWM. Obviously the majority of the bandwidth is provided by the SWM. Therefore, as R_o decreases, the contribution of the SWM to instability increases and so does the bandwidth. On the other hand, the normalized growth rate decreases from 0.77% for the pure IWM to 0.36% for the mixed mode. The maximum growth rate decreases as the contribution of the SWM via R_o reduction is increased. If the high gain as well as the wide bandwidth is desired, then some compro-

mise must be made in reducing the beam center radius.

We conclude this section by summarizing the following. First, the SWM intermixes with the IWM by reducing the beam radius from $R_o/R_o^o = 0.9$ to $R_o/R_o^o = 0.5$. By an appropriate reduction of the beam radius, the bandwidth of the mixed mode can be more than twice of that for the pure IWM. Second, because of the presence of a dielectric material with the large dielectric constant ($\varepsilon \sim 15$), a considerable range of the SWM can freely propagate (i.e., $\omega > ck/\varepsilon^{1/2}$), thereby eliminating difficulties associated with the pure SWM. However, the maximum growth rate of instability for the mixed mode operation is substantially less than that for the IWM. In the next section, we will examine the influence of the mixed mode on the perturbed field profile.

IV. PERTURBED FIELD PROFILES

In this section we will examine the perturbed field profiles in terms of the beam center location. The field profile reveals the nature of the instability and the field energy distribution across the cross section. For the IWM, the perturbed field profile is almost identical to that for the beam-free waveguide mode. On the other hand, for the SWM, it is highly localized at the beam center location (see Appendix). In this regard, we can identify the dominant instability mode by examining the field structure. Moreover, from the field profile, we can compute the amount of the electromagnetic field energy contained in the dielectraic layer, so that the heat dissipation through the layer can be quantitatively compared.

Within the context of the thin beam approximation[1] the perturbed fields for the azimuthally symmetric TE mode are given by (within a normalizing factor)

$$E_{\theta 1} = \begin{cases} J_1(x), & 0 \le r < R_- = R_o, \\ \dfrac{J_1(x_o)}{D}\,[B_2 J_1(x) - B_1 N_1(x)], & R_w \ge r > R_+ = R_o, \\ \dfrac{2}{\pi}\,\dfrac{J_1(x_o)}{D}\,[N_1(y_c)J_1(y) - J_1(y_c)N_1(y)], & R_w \le r \le R_c, \end{cases} \tag{10}$$

$$B_{r1} = -\frac{ck}{\omega} E_{\theta 1}, \quad B_{z1} = -\frac{ic}{\omega}\frac{1}{r}\frac{d}{dr}(rE_{\theta 1}) \tag{11}$$

Here the quantities D, B_1, B_2, x and y are defined by Eqs. (5)-(7). In the slow region ($\omega < ck$), the Bessel functions J and N become the combination of the modified Bessel functions I and K for $0 \le r \le R_w$. It is interesting to note that when $R_o = R_w$, the field eqs.(10)-(11) describe the beam-free waveguide mode. We, therefore, expect that when the beam center (R_o) is placed near the inner dielectric wall (R_w), the electron beam does not appreciably change the beam-free waveguide (the IWM).

In Fig. 5, the profiles of the transverse fields are shown for several beam locations at the wave number $k = 4.0\ \omega_c/c$. The other parameters are identical to those in Fig. 4. The arrows indicate the beam center locations. The fields are normalized such that $\int_o^{R_c} [\varepsilon_j E_{z1}^2 + B_{\theta 1}^2]\, r dr = R_c^2$. Here $\varepsilon_j = 1(\varepsilon)$ for $0 \le r \le R_w$ ($R_w \le r \le R_c$). We note that the chosen wave number $k = 4.0\ \omega_c/c$ ($\omega = 1.7\ \omega_c$) corresponds to the border line between the IWM and the SWM [see Figs. 3 and 4(a)]. It is evident from Fig. 5 that for $R_o/R_o^{\,o} = 0.9$, the field structure resembles the beam-free waveguide mode indicating the dominance of the IWM contribution, whereas for $R_o/R_o^{\,o} = 0.5$, it is localized near the beam exhibiting a dominant SWM influence. The contribution of the SWM increases as R_o decreases from the pure IWM ($R_o/R_o^{\,o} = 0.9$) to the mixed mode ($R_o/R_o^{\,o} = 0.5$). Figure 5 also shows that the field con-

centration in the dielectric layer reduces as R_o decreases. To illustrate its dependence on the wave number k, Fig. 6 shows the field structure for the mixed mode ($R_o/R_o^o = 0.5$, shown by the arrow) at several values of the axial wave number. It is apparent from Fig. 6 that at a low axial wave number (e.g., $kc/\omega_c = 1.5$) the field is nearly the same as that of the beam-free waveguide. On the other hand, as k increases the field becomes more localized at the beam location, indicating the increasing contribution of the SWM. Especially at $kc/\omega_c = 10.0$, the field is very highly localized near the beam location, i.e., $E_{\theta 1} \sim \delta(R-R_o)$. The transition from the IWM to the SWM occurs near $kc/\omega_c \sim 3.5$, $\omega/\omega_c \sim 1.6$ as shown in Figs. 3 and 4(a). We therefore conclude from Figs. (5)-(6), that the contribution of the SWM can be enhanced by decreasing R_o and by increasing k.

We now evaluate the field energy contained in the dielectric layer. Although our model does not include the detailed loss mechanism, we can relatively examine the heat dissipation in the dielectric layer by comparing the total wave energy stored in the layer when the beam radius is reduced from $R_o/R_o^o = 0.9$ to $R_o/R_o^o = 0.5$. In Fig. 7 the ratio of the wave energy in the dielectric layer ($\mathcal{E}_D$) to that in the total cross section ($\mathcal{E}_T$) is given as a function of the wave frequency for various beam locations. Here the field energy per unit axial length $\mathcal{E}$ is defined by $\mathcal{E} \equiv \frac{1}{2}\int(\epsilon_j \underset{\sim}{E}_1^2 + \underset{\sim}{B}_1^2)rdr$. The energy in the dielectric layer is large ($\sim$ 80%) in the IWM region (i.e., small k) and is negligible in the SWM region (i.e., high k). Also for given k, the layer energy decreases as R_o decreases except for k in the IWM region. Reminding that SWM contribution increases as R_o decreases and as k increases, the reduction of the dielectric layer energy for the mixed mode is obviously due to the enhanced SWM contribution via its tendency to localize the field at the beam location (see Figs. 5-6). In Fig. 7 the vertical arrows indi-

cate the edges of the bandwidth ($k_{\pm}$) for each value of the beam radius R_o. Assuming that the intensity of the input wave is the same over the whole region of the bandwidth, we compute the bandwidth-integrated energy $W = \int_{k_-}^{k_+} \mathcal{E}\, dk$ where $k_+(k_-)$ is the upper (lower) marginal point of the bandwidth. The ratio of the bandwidth integrated energy in the dielectric layer ($\bar{W}_p$) to that in the total cross section (W_T) is plotted versus the beam location R_o in Fig. 8. The quantity W_D represents the total field energy in the dielectric layer when the input wave with the same amplitude is sent over the entire bandwidth. The reduction of W_D/W_T with decreasing value of R_o is obvious. When R_o is reduced, so does $\mathcal{E}_D/\mathcal{E}_T$ (Fig. 7), considerably increasing the bandwidth [Fig. 4(a)] which includes a large portion of high k value with negligible $\mathcal{E}_D$ (Fig. 7). The ratio W_D/W_T is reduced from 83% for the pure IWM (i.e., $R_o/R_o^o = 0.9$) to 24% for the mixed mode (i.e., $R_o/R_o^o = 0.5$). Therefore, for example, if the dielectric layer withstands 50 KW of the wave power for the pure IWM operation, it can withstand 175 KW (3.5 times) of the power for the mixed mode.

In this section we have examined the perturbed field profile. As the beam center location is reduced toward the axis, we find that the contribution of the SWM is enhanced, increasing the bandwidth and decreasing the field energy in the dielectric layer. The nature of the SWM which localizes the field at the beam location is responsible for the reduction of the field energy in the dielectric layer.

V. CONCLUSION

We have investigated the possible bandwidth broadening effect by mixing the short wavelength mode with the usual intermediate wavelength mode in a dielectric gyrotron. The increasing participation of the SWM is provided by locating the beam center away from the inner wall of the dielectric

layer and toward the axis. The resulting bandwidth of the mixed mode gyrotron is wider than that for either of the two individual slow wave modes. It is found that the enhanced SWM contribution is responsible for the almost twice enhancement of the bandwidth. Up to 90% of the bandwidth[8] is possible at small axial momentum spread ($\Delta \lesssim 1\%$).

The mixed mode operation eliminates in part the difficulties arising from the individual utilization of the two slow waves. The presence of the dielectric layer (i.e., the IWM) makes the propagation of the input wave possible for the SWM operation. On the other hand, the characteristics of the SWM, namely the localization of the perturbed fields at the beam location, greatly reduces the field energy in the dielectric layer. Therefore, the mixed mode gyrotron withstands the heat dissipation in the dielectric layer for more effectively than the IWM operation. In particular the bandwidth-integrated energy in the dielectric layer for the mixed mode is a factor of 3.5 smaller than that for the IWM operation.

Finally, it is reiterated that this mixed mode operation is very much susceptible to the axial momentum spread, and thus it is only possible at small spread ($\Delta \lesssim 1\%$).

ACKNOWLEDGMENT

This research was supported in part by an Independent Research Fund at the Naval Surface Weapons Center, and in part by the Office of Naval Research and the Naval Electronic Systems Command.

APPENDIX

PHYSICAL MECHANISM OF INSTABILITY FOR THE SHORT WAVELENGTH MODE

In this Appendix, we present a simplified model describing the instability mechanism responsible for the short wavelength mode (SWM). Since its mathematical descriptions have been already presented in terms of the dispersion relation [Eq. (3), Sec. II], it is sufficient here only to illustrate existence of the SWM instability in a simple sketchy description. Introducing a small perturbation to the equilibrium in a simple geometry, we examine the response of the system whether it enhances (unstable) or reduces (stable) the perturbation.

In our simple model, the beam electrons are assumed to be cold and to have same canonical angular momentum. Therefore, in a frame moving at the axial beam velocity, all electrons are on the cyclotron orbit with the same Larmor radii r_L and the same transverse velocity $v_\perp$ as shown in the first diagram of Fig. 9(a). Thus in equilibrium the motion of the electrons are purely transverse. Three representative planes of the electrons are shown in the second diagram of Fig. 9(a). Each electron on the plane experiences the attractive forces from the neighboring electrons in the axial direction because of the currents in the same direction. However, this axial force vanishes due to the symmetry. The force acting on the electron at B_1 in the graph, for example, due to the electron at A_1 cancels that due to the electron at C_1. Assuming a small perturbation as shown in the third diagram of Fig. 9(a), the plane B_1-B_2 is tilted with a small angle $\delta\phi$ with y axis (B_1'-B_2'). Then the axial force on the electron at B_1' is positive since $\overline{A_1B_1'} > \overline{B_1'C_1}$. Similarly there is a net axial force on B_2' with the same magnitude but opposite direction. This results a torque on the plane B_1'-B_2'

that further increases the perturbation. For a small tilt angle satisfying $\delta\phi \ll 1$, we can approximate the electron motion as that of the permanent magnetic dipole moment. At equilibrium the dipole moment $\underline{M}$ is in the opposite direction of $B_o \hat{e}_z$ as shown in Fig. 9(b). If we introduce the perturbation angle $\delta\phi = \delta\phi_o \sin kz$, then the planes of the transverse electron orbit and the associated dipole moments can be expressed as Fig. 9(c). Since the magnitude of the dipole moment $M = |\underline{M}|$ is adiabatically invariant up to the order of $\delta\phi_o$ ($\ll 1$), the tilted dipole moment is given by $\underline{M}(\delta\phi) = M_z \hat{e}_z + \delta My\, \hat{e}_y \simeq -M \hat{e}_z + M\delta\phi\, \hat{e}_y$. The y-component of the dipole moment δM_y and the tile angle $\delta\phi$ are shown in Fig. 9(d). Computing the torque $\underline{N} = \underline{M} \times \underline{B}$. We obtain

$$
\begin{aligned}
N_x &= M_z\, \delta B_y^m + \delta M_y (B_o + B_z^m) \\
&= MB_o\, \delta\phi \left[1 + \frac{B_z^m}{B_o} - \frac{(\delta B_y^m/\delta\phi)}{B_o} \right] \\
&\simeq MB_o\, \delta\phi
\end{aligned}
\qquad \text{(A-1)}
$$

where B_z^m and δB_y^m refer to the magnetic fields associated with the tilted dipole moment $\underline{M}(\delta\phi)$. The last approximation in Eq. (A-1) results from the tenuous beam assumption ($\nu \ll 1$), since $|B_z^m/B_o| \sim |(\delta B_y^m/\delta\phi)/B_o| \sim o(\nu)$. The resulting N_x is drawn in Fig. 9(e). Note that when $N_x > 0$ (<0), the plane of the transverse electron orbit motion is rotating in the clockwise (counter-clockwise) direction in the y-z plane as shown in the graph. As we have seen in Fig. 9(a), the resulting torque N_x reinforces the initial perturbation angle, thereby resulting an instability.

We have shown the existence of the SWM instability with a magnetostatic concept of the magnetic dipole moment. It is interesting to note that the beam response in the transverse direction is paramagnetic (i.e., $\delta M_y \delta B_y^m > 0$),

although overall diamagnetism is preserved in the axial direction ($M_z B_o < 0$). The instability is derived essentially from this paramagnetic property in the transverse direction. The concept of the magnetic dipole moment yields another important result. The perturbed magnetic field from the tilted electron plane, δB_y exhibit the dipole property when $|y|$ becomes large. That is, as the point of observation is far removed from the electrons, the perturbed magnetic field δB_y rapidly decreases. In this regard, the perturbed magnetic field δB_y is concentrated near the beam location.

We now clarify the relation of this simple model with that given in the text. When the origin is replaced by R_o [see Fig. (1)], then we have $x \to \theta$ and $y \to r$. Also since the SWM is prominent when $\omega << ck$, the electric field $E_{\theta 1}$ can be neglected $[|E_{\theta 1}/B_{r1}| = \omega/ck << 1$, Eq. (11)]. Thus the magnetostatic description with $\omega \to 0$, and $E_{\theta 1} \to 0$ is justified. The effect of the finite geometry (i.e., finite R_c) is not as important for the SWM as it is for the LWM. The LWM growth rate is enhanced (from $\omega_i \sim \nu^{1/2}$ to $\nu^{1/3}$) by synchronizing the beam mode with the waveguide mode with finite geometry. For the SWM, the finite geometry further localizes the dipole field in the infinite space toward the beam location. This localization of the field is obvious in Figs. (5)-(6).

REFERENCES

1. J.Y. Choe, H.S. Uhm, and S. Ahn, J. Appl. Phys. in press (1981).
2. See the Proceedings of the Conference on Defence Department Programs in Gyrotron Research and Development, Naval Research Lab Memo. Rep. XXXX (April 1981); (a) On gyrotron gun studies by J.M. Baird and P. Ferguson (b) On dielectric gyrotron programs by S.Y. Park and J. Choe and (c) Comments on the dielectric heating by P. Ferguson.

3. H. Keren, J.L. Hirshfield, S.Y.Park, K.R. Chu, J.M. Baird "Design of a slow wave cyclotron wave amplifier," Proceedings on the Fifth International Conference on Infrared and Millimeter Waves, pp 96-97, October 6-10, 1980.

4. H.S. Uhm and R.C. Davidson, Phys. Fluids 23, 2538 (1980).

5. H.S. Uhm, R.C. Davidson, and K.R. Chu, Phys. Fluids 21, 1877 (1978).

6. K.R. Chu, Phys. Fluids 21, 2354 (1978).

7. J.Y. Choe and S. Ahn, IEEE Trans. Electron Devices ED-28, 166 (1981).

8. The bandwidth defined here corresponds to the 7.5 dB total gain for the 3 dB power loss. For the total gain of 15 dB, the bandwidth drops to 60%.

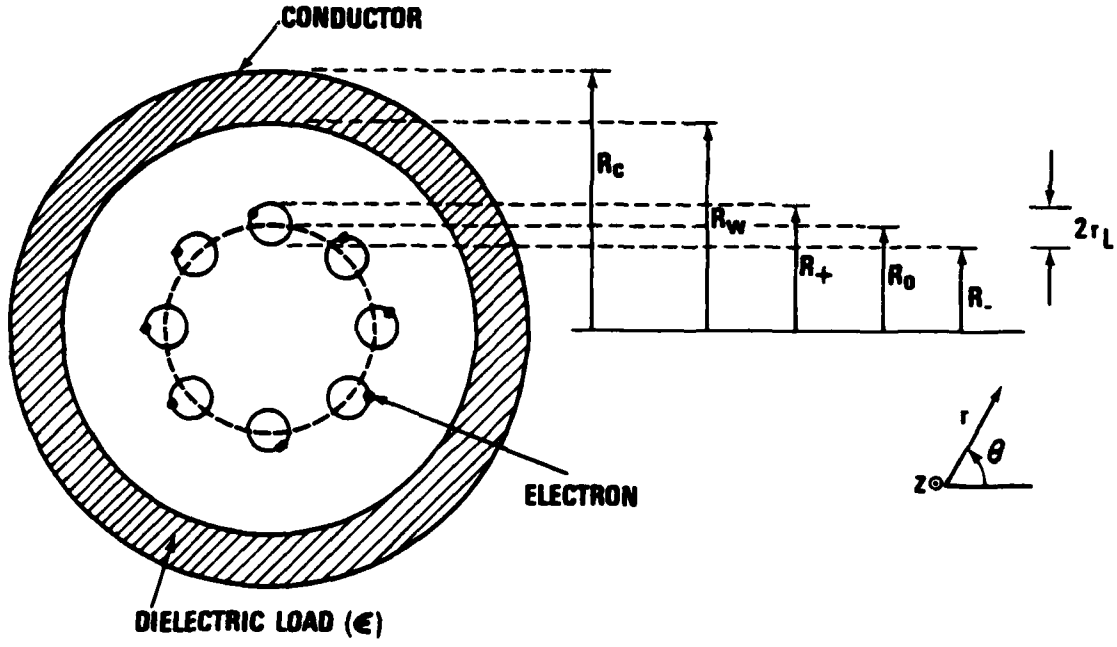

Fig. 1 — Configuration of a dielectric loaded gyrotron. A dielectric material (ϵ) is filled from its inner radius R_w to the perfect conductor at R_c. The hollow electron beam is confined within $R_- < r < R_+$ with beam radius $R_0 = (R_- + R_+)/2$.

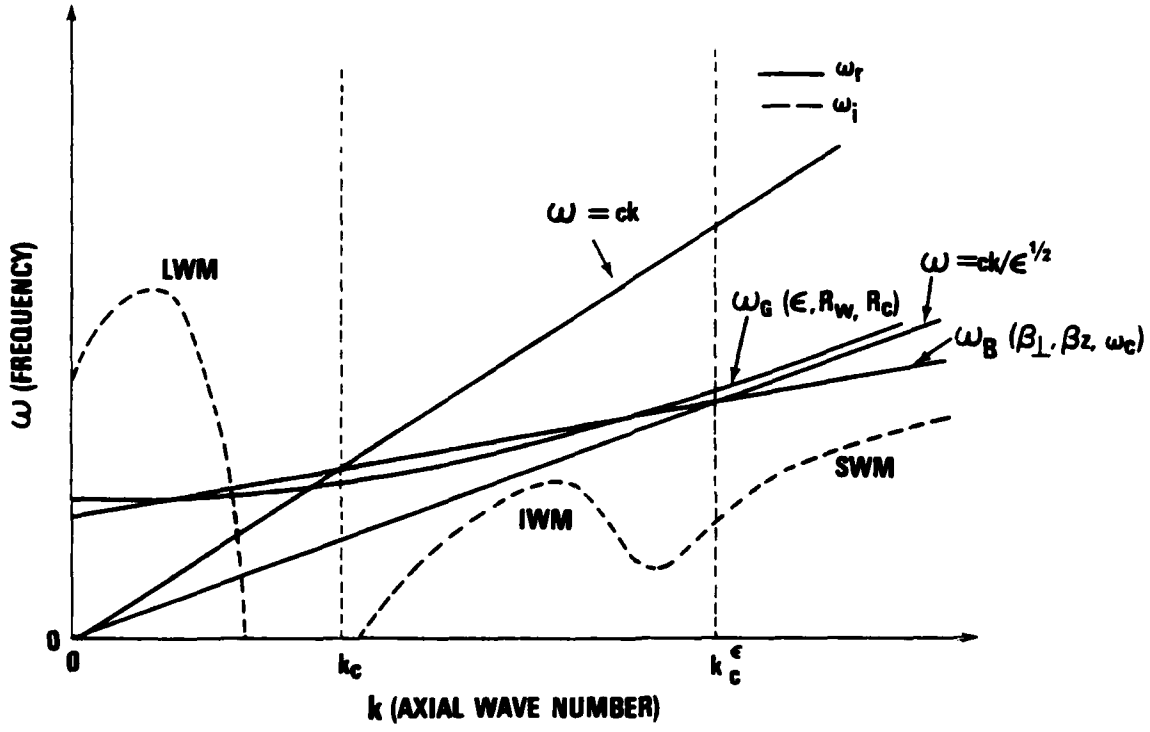

Fig. 2 — Schematic dispersion and growth rate curves versus the axial wavenumber. The dispersion curves (solid) for the beam mode (ω_B), the dielectric waveguide mode (ω_G) and the two characteristic speeds (ck and $ck/\epsilon^{1/2}$) are shown. The growth rate curve (broken) shows three unstable modes (LWM, IWM and SWM) identified by the axial wabe number. The distinguishing wave number k_c and k_c^{ϵ} are the interesting points of $\omega = \omega_B$ with $\omega = ck$ and $\omega = ck/\epsilon^{1/2}$, respectively.

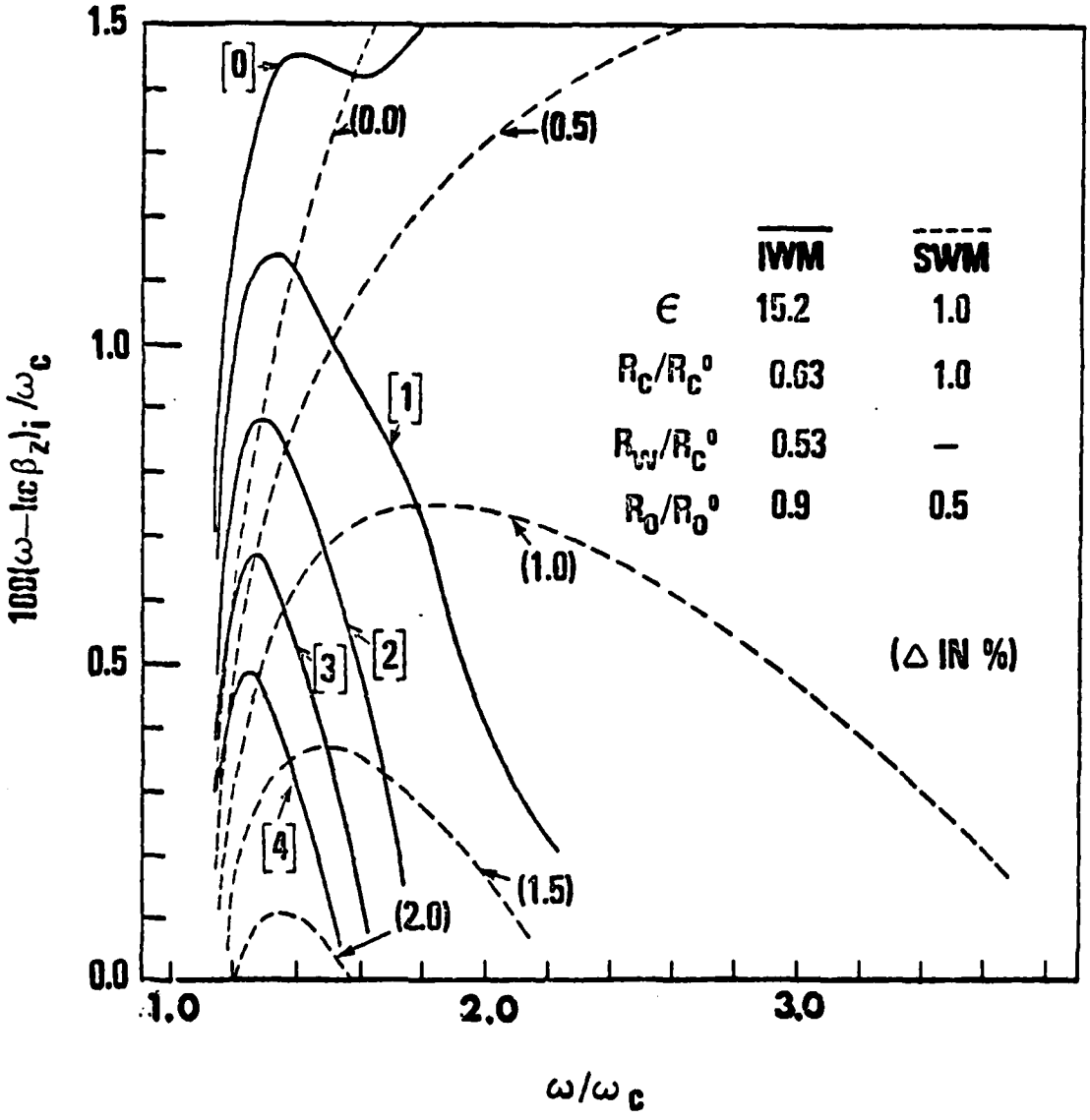

Fig. 3 — Plots of the gain versus the wave frequency at several values of the axial velocity spread (Δ) for the IWM and the SWM. Note the different physical parameters for each mode. Other parameters are given in Eqs. (8)-(9). ω_c is the cyclotron frequency.

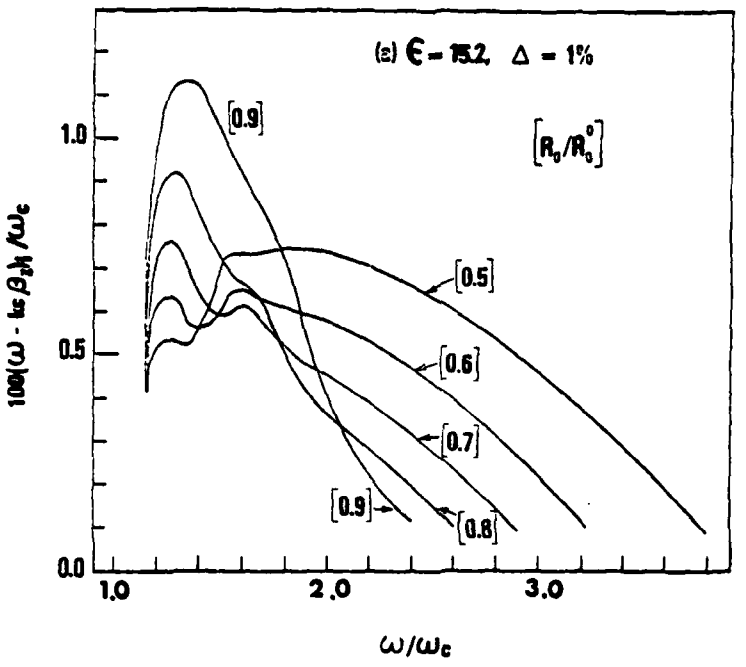

(a)

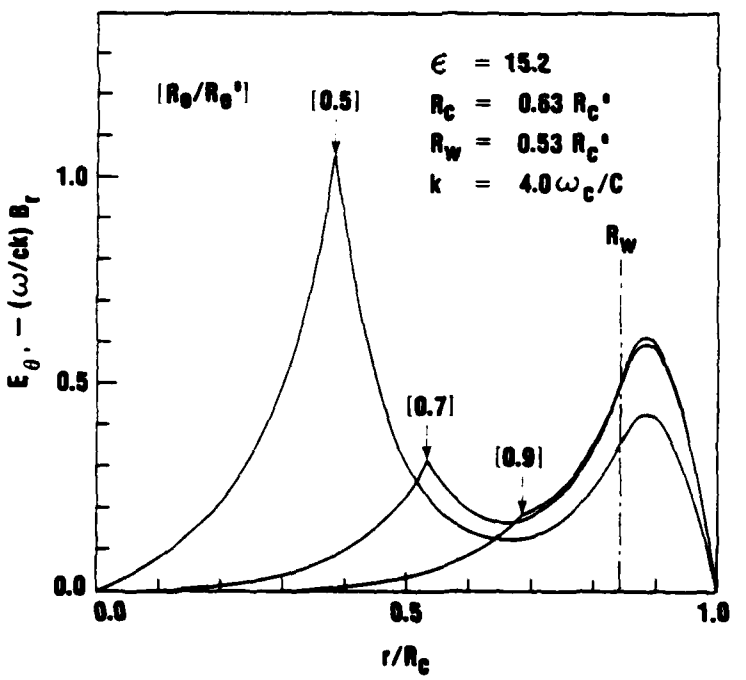

(b)

Fig. 4 — Mode mixing via variation of the beam location (R_0). The parameters otherwise are identical to those of the IWM in Fig. 3 and Eq. (8). The axial momentum spread is assumed to be 1%. (a) Plots of the gain versus the wave frequency for several values of the beam location. The SWM contribution is enhanced as R_0 decreases. (b) Plots of the normalized bandwidth and the maximum growth rate versus the beam center location.

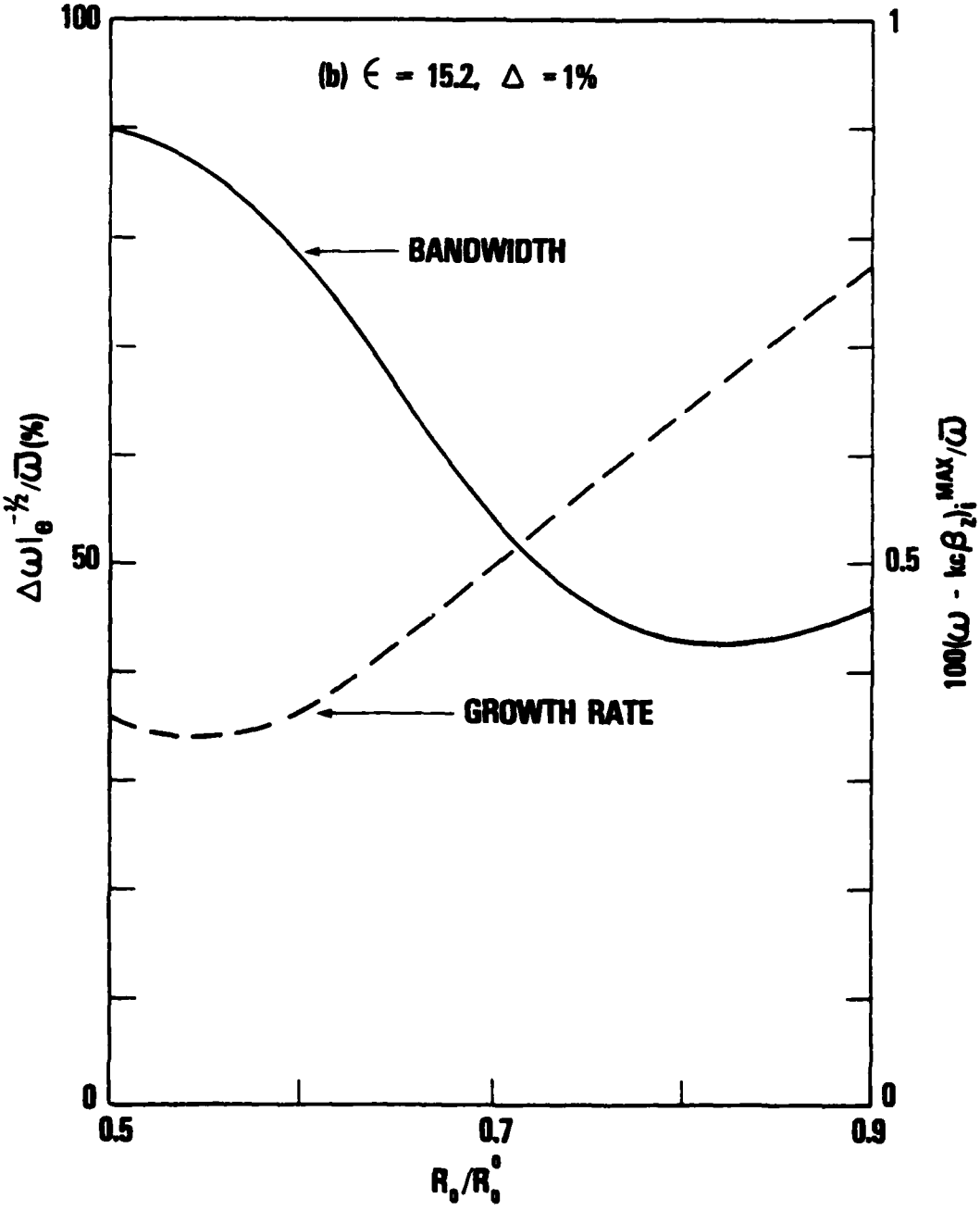

Fig. 5 — Normalized transverse field profiles with variation of the beam location at the given parameters and at the given wave number. The vertical arrows indicate the beam center locations.

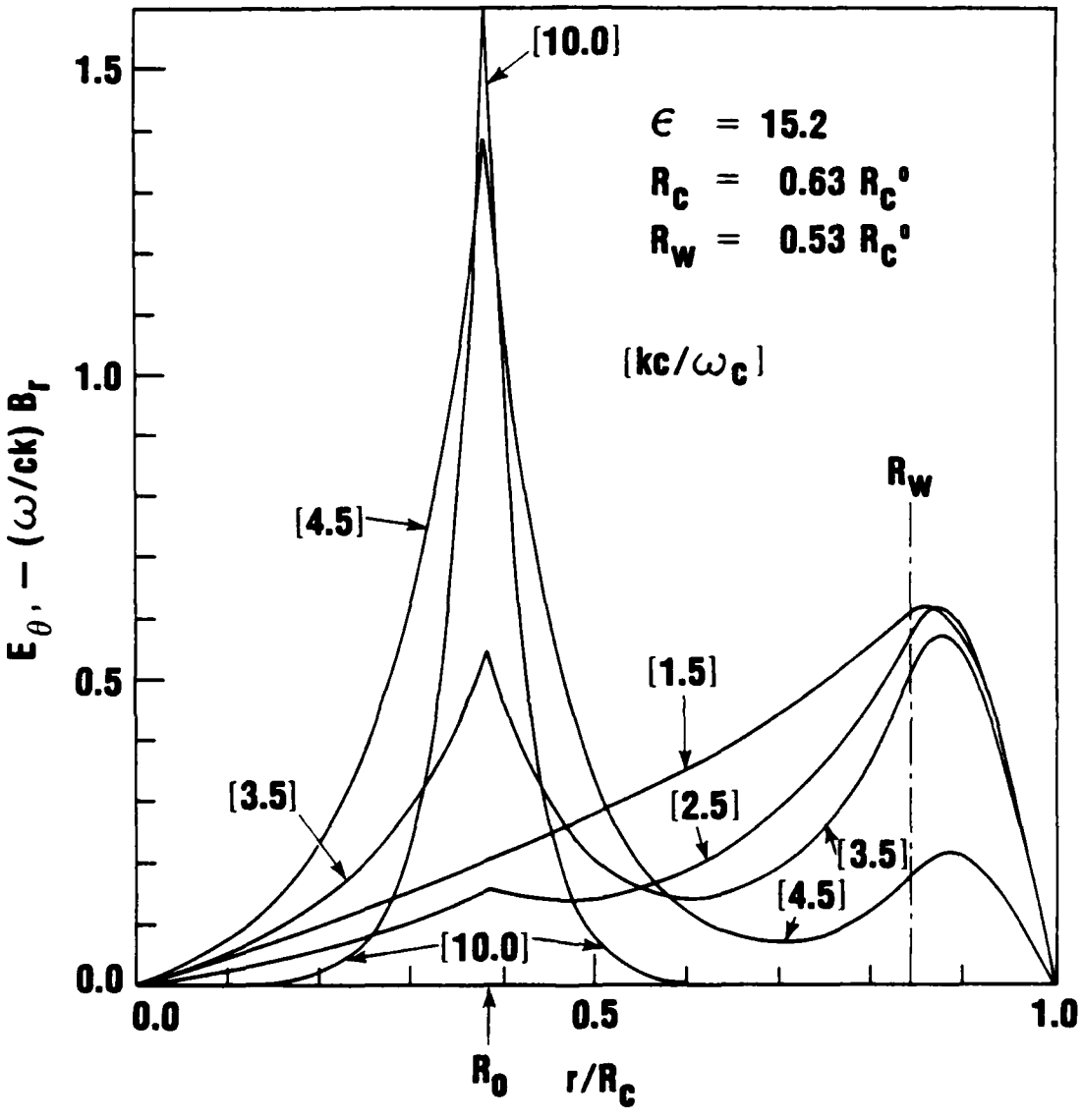

Fig. 6 — Dependency of the field profiles on the wave number (or the frequency) at the mixed mode operation (R_0/R_0^o=0.5). The beam location is shown by the arrow in the bottom.

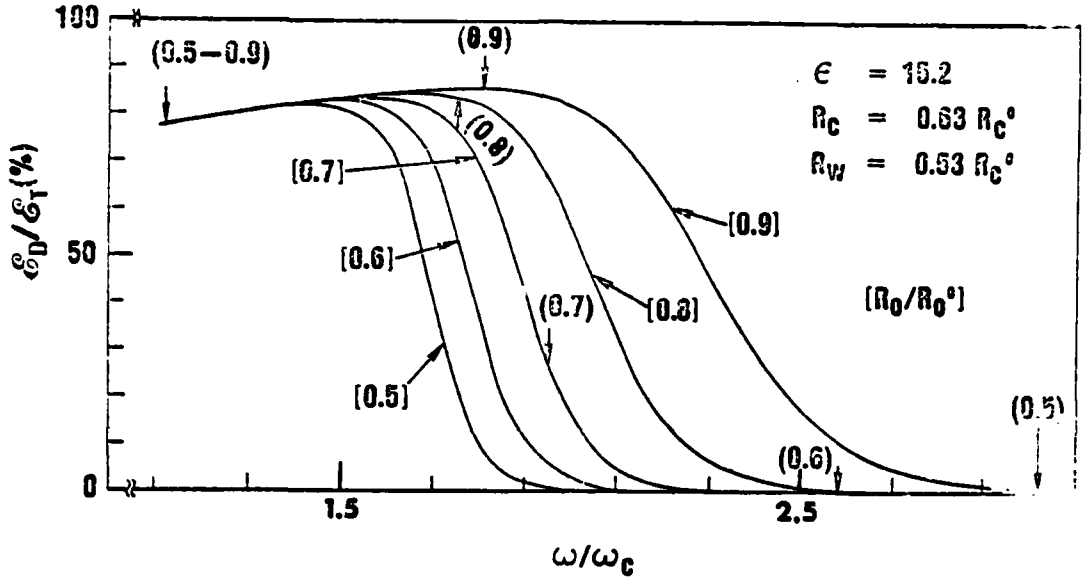

Fig. 7 — Plots of $\mathcal{E}_D/\mathcal{E}_T$ versus the frequency at several values of the beam center location. The vertical arrows indicate lower and the upper boundaries of the bandwidth for each case.

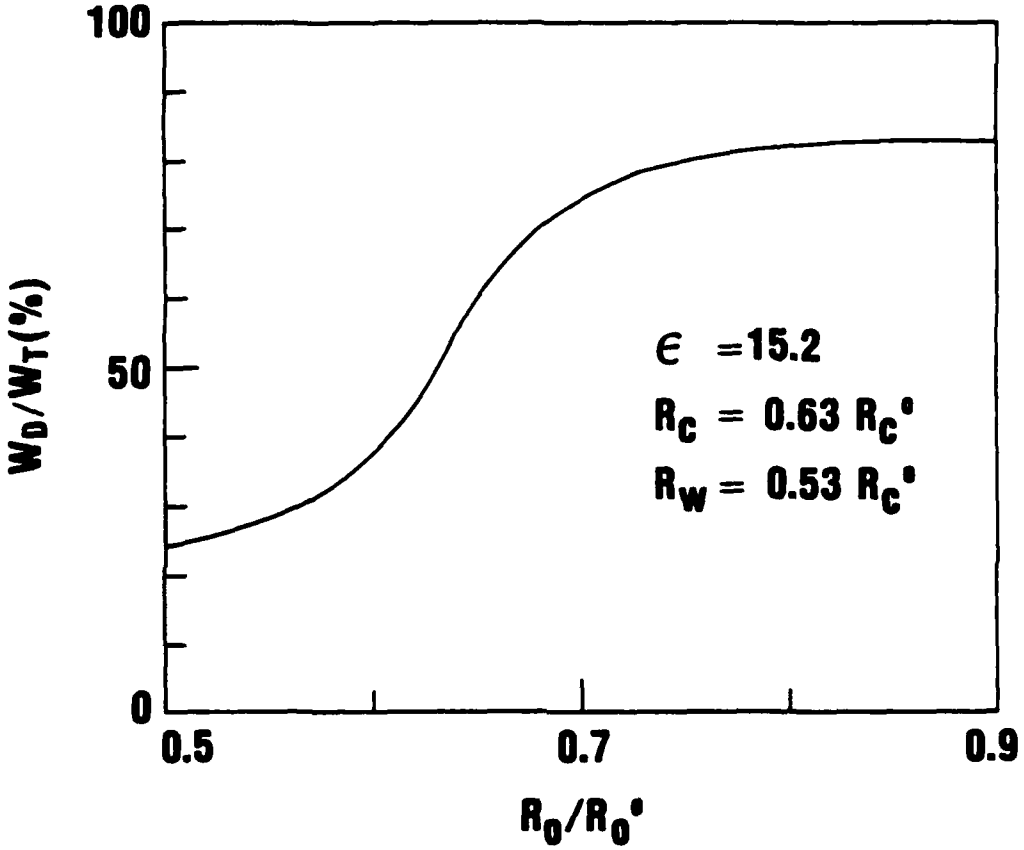

Fig. 8 — Plots of W_D/W_T versus the beam location

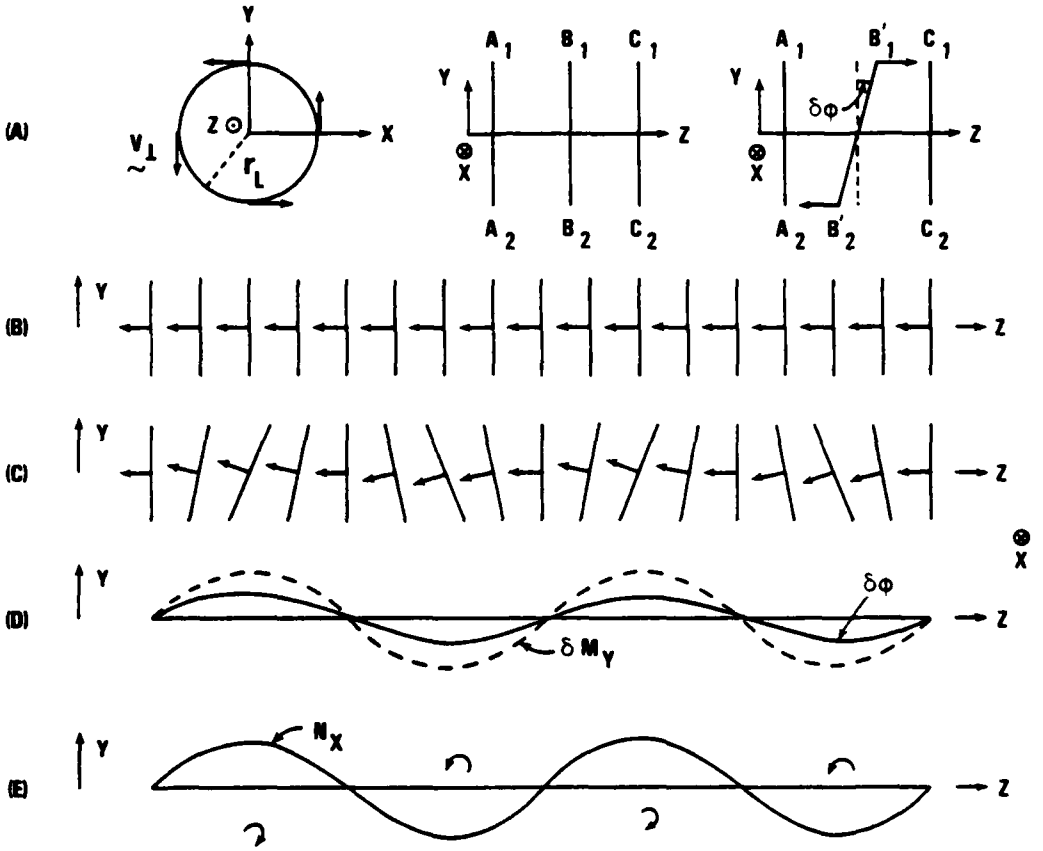

Fig. 9 — Schematic description of the SWM instability

(a) The x-y plane (first) and the y-z plane (second projections of the equilibrium electron orbit, and the perturbed projections in y-z plane (third).
(b) Equilibrium planes of motion and the magnetic dipole moments
(c) Perturbed planes of motion and the magnetic dipole moments
(d) The tilt angle $\delta\phi$ and the y-component of the magnetic dipole moment δM_y
(e) The resulting torque N_x

END

DATE
FILMED
6-81

DTIC